Available online at www.sciencedirect.com
ScienceDirect
Trans. Nonferrous Met. Soc. China 34(2024) 3170−3184
Transactions of Nonferrous Metals Society of China
www.tnmsc.cn

Modeling of recrystallization behaviour of AA6xxx aluminum alloy during extrusion process

Marco NEGOZIO[1], Antonio SEGATORI[2], Riccardo PELACCIA[3], Barbara REGGIANI[3,4], Sara Di DONATO[5], Lorenzo DONATI[5]

1. University of Parma - Department of Engineering and Architecture, Parco Area delle Scienze, 181/A, 43124 Parma, Italy;
2. Hydro, Innovation and Technology, Myrkärrsvägen 1, 612 31 Finspång, Sweden;
3. DISMI Department of Sciences and Methods for Engineering, University of Modena and Reggio Emilia, Via Amendola 2, 42122, Reggio Emilia, Italy;
4. InterMech - MO.RE – University of Modena and Reggio Emilia, Piazzale Europa 1, Reggio Emilia 42124, Italy;
5. DIN Department of Industrial Engineering – University of Bologna, Viale Risorgimento 2, 40136, Bologna, Italy

Received 20 July 2023; accepted 14 November 2023

Abstract: An innovative approach was introduced for the development of a AA6063 recrystallization model. This method incorporated a regression-based technique for the determination of material constants and introduced novel equations for assessing the grain size evolution. Calibration and validation of this methodology involved a combination of experimentally acquired microstructural data from the extrusion of three different AA6063 profiles and results from the simulation using the Qform Extrusion UK finite element code. The outcomes proved the agreement between experimental findings and numerical prediction of the microstructural evolution. The trend of the grain size variation based on different process parameters was accurately simulated, both after dynamic and static recrystallization, with an error of less than 25% in almost the whole sampling computations.

Key words: recrystallization simulation; aluminum alloy extrusion; finite element method; microstructure prediction

1 Introduction

The control of the microstructure evolution during extrusion of AA6xxx aluminum alloys is of primary importance to improve the material properties [1]. To date, due to the complexity of the recrystallization kinetics, the relationship between extrusion parameters and grain structure evolution is still not fully understood [2].

During the extrusion of AA6xxx aluminum alloys, three different types of profile microstructures can be obtained: fibrous, recrystallized, and partially recrystallized [3]. In the fibrous structure, grains are lengthened through the extrusion direction, while in the recrystallized structure, a single average diameter can be used to describe the size of grains, which have spheroidal shapes. Moreover, the partially recrystallized microstructure, often found in medium-strength 6xxx aluminum alloy profiles (6082, 6061, etc.), presents recrystallized grains near the profile surface while the inner part of the structure remains fibrous [4].

The microstructure evolves throughout the entire extrusion process as a result of the applied deformation and two primary mechanisms [5,6] for recrystallization: dynamic (DRX) and static (SRX).

Corresponding author: Marco NEGOZIO, Tel: +39-052190-6029, E-mail: marco.negozio@unipr.it
DOI: 10.1016/S1003-6326(24)66600-8

As a result of the hot deformation applied during the extrusion process, the grains change their shape starting in the billet material, where the grain is recrystallized as a result of the homogenization process. Consequently, the initially spheroidal billet grains turn into a fibrous configuration in the profile. During this evolution, the dynamic recrystallization triggering conditions may occur. In high stacking fault energy materials (HSFE, as aluminum alloys), different DRX kinetics are still under discussion in the research community [7]: the Geometric Dynamic Recrystallization (gDRX), the Continuous Dynamic Recrystallization (cDRX) and the Joint Dynamic Recrystallization (jDRX). The gDRX and cDRX theories were proposed by MCQUEEN et al [8] and GOURDET and MONTHEILLET [9], respectively. The first claimed that, when the grain thickness reduces during the deformation till it becomes 2−3 times the subgrain size, the original grain splits in two new grains ("pinch-off"). The second suggested a mechanism of new grain formation related to the evolution of the misorientation angle of subgrains, which increases till the LAGB (low angle grain boundaries, which surround the subgrains within the grain) become HAGB (high angle grain boundaries, which surround the grains) [10]. Moreover, a joint theory was suggested called jDRX. This theory was proposed by de PARI and MISIOLEK [11] and investigated by DONATI et al [5], and it combines the gDRX and cDRX into a unified model validated in the AA6061 hot rolling process. Following the extrusion process and profile formation, static recrystallization may occur, resulting in additional microstructural changes via the formation and growth of new grains. This transformation leads to a complete replacement of the fibrous structure with a static recrystallized one [12]. Several authors investigated the SRX in the hot deformation processes of 6xxx aluminum alloys, focusing attention on how the different material and process parameters may affect the recrystallization behaviour. SELLARS and ZHU [13] proposed a model able to evaluate internal variables such as dislocation density, subgrain size, and subgrain misorientation angle and their relation to static recrystallization. VATNE et al [14] calculated the SRX grain size as a function of the nucleation, which depends on different contributions: the particle-stimulated nucleation, the cube band nucleation, and the grain boundary nucleation. The evaluation of these three nucleation contributions was further investigated by EIVANI et al [15] in the hot deformation of Al−4.5Zn−1Mg aluminum alloy.

Recent developments have demonstrated the efficiency of finite element codes in modeling the thermal and mechanical dynamics that occur during extrusion. HE et al [16] studied the effect of pockets in the porthole die on extrusion load, exit temperature and material flow during the extrusion of a AA6061 aluminum alloy profile by using the DEFORM-3D software. HE et al [17] investigated the field distributions of strain rate, stress, temperature and velocity through the Altair HyperXtrude fem code. FERESHTEH-SANIEE et al [18] performed the analysis of the effect of die design on the extrusion load through experiment and FEM simulation. YI et al [19] used the finite element modeling (Arbitrary Lagriangian−Eulerian algorithm) to solve the defects of bottom concave during the extrusion of complex hollow profiles. YI et al [20] also carried out the investigation of the isothermal extrusion of AA6063 hollow profile using incremental proportional-integral-derivative (PID) control algorithm and finite element simulations. ZHANG et al [21] and KHAN et al [22] used different crystal plasticity models with FEM codes to simulate the texture evolution during the extrusion of a AA6463 aluminum alloy and the single crystal deformation in compression tests of pure aluminum (99.999% in purity), respectively. PELACCIA et al [23] simulated the liquid nitrogen cooling in aluminum alloy extrusion for the cooling channel design optimization by using the Comsol finite element code. EIVANI and ZHOU [24] carried out FEM simulations to investigate the formation of the peripheral coarse grain (PCG) during the hot extrusion of an AA7020 aluminum alloy. The study continued in 2020, with further development in the study of PCG kinetics [25]. MAHMOODKHANI et al [26] investigated the effect of different die geometries on the micro-structure of Al−Mg−Si−Mn alloy extruded profiles, both experimentally and numerically using FEM simulation. These studies have undergone testing and validation to enable simulation of some of the key factors that control recrystallization, including stresses, temperature, strain, and strain rate.

In this context, the primary objective of the current work is to propose a reliable approach for

developing recrystallization models specifically tailored for 6xxx aluminum alloys. The methodology includes collection of experimental data on microstructural evolution during the extrusion of a specific 6XXX aluminum alloy, simulating the investigated extrusion process using FEM simulations, and developing a recrystallization model optimized for describing the microstructural behavior of the analyzed 6xxx alloy. The recrystallization model utilized in this study was taken from NEGOZIO et al [27] and further enhanced by incorporating two new equations for calculating internal dislocation density and misorientation angle. For the experimental campaign, an AA6063 aluminum alloy profile was extruded with a wide range of process parameters under strictly monitored conditions to validate the FEM simulation. Using the acquired experimental data, the proposed model was tailored for the examined AA6063 alloy and then implemented within the FEM code Qform Extrusion to predict the AA6063 microstructure. The accuracy of the prediction was verified by comparing the grain size predictions to the microstructural data also acquired on two additional industrial extruded AA6063 profiles. The primary aim of this work is to introduce and validate a robust methodology for characterizing the microstructural evolution of a studied 6xxx aluminum alloy during hot forming processes. The ultimate goal is to optimize the microstructure of the final product and, thereby, enhance its properties.

2 Methodology

The proposed methodology aims to develop an optimized recrystallization model for the 6xxx aluminum alloy under investigation (Fig. 1). The work of NEGOZIO et al [27] provided the base for the initial 6xxx recrystallization model, which allowed for the prediction of statically and dynamically recrystallized grain size and recrystallization thickness during hot forming procedures. In order to achieve this optimization, the required material constants must be calculated. These values are derived from a comprehensive set of experimental and numerical data obtained through appropriate experiments and simulations. The experiment involves the extrusion of profiles with various process parameters (i.e. different ram speeds, billet pre-heating temperatures) and the acquisition of all microstructural data. Moreover, FEM simulations of the extrusion are conducted to extract the temperature, strain rate, and strain data from the simulations. These simulation results are then integrated with the data obtained from experiments, and a regression algorithm is employed to optimize the recrystallization model. After the investigated alloy recrystallization model has been developed, it is applied as post-processing to FEM simulations to predict the microstructure after hot forming processes.

3 Experimental

The AA6063 profile was extruded at the Hydro ETC in Finspång (Sweden) with a 10 MN extrusion press. In Fig. 2, the geometries of profile and die are shown.

In detail, the experiment involved the extrusion of 20 billets: a combination of four ram speeds (1.1, 2.1, 9.2 and 10.4 mm/s) and two different billet temperatures (420 and 490 °C) was tested. Through the use of a pyrometer, the profile

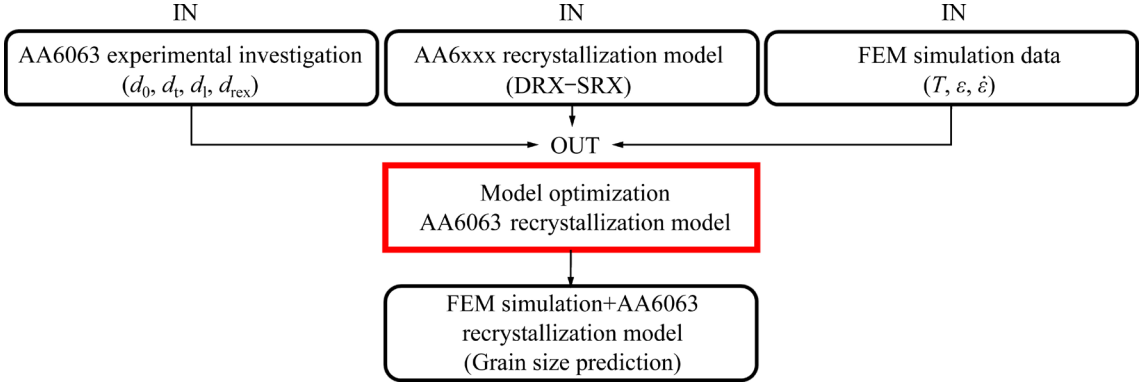

Fig. 1 Methodology for 6xxx recrystallization model optimization

temperature trends at the exit of the extrusion die were recorded, and the obtained data were used to validate the numerical simulations. In order to collect values of the average grain size of the profiles, samples were ground, polished, and then etched with Barker's reagent (etching parameters: 40 V dc, 4 min; reagent composition: 15 mL HBF4, 750 mL H_2O). For each profile, two different microstructures are shown, one taken from the beginning of each extruded length ("Front" in Fig. 3) and one from the end ("Back" in Fig. 3).

Figures 3(a, b) represent the grain structures that result from the extrusion made with a billet temperature of 420 °C and a ram speed of 1.1 mm/s. Figures 3(c, d) represent the grain structures resulting from the extrusion made with a billet temperature of 490 °C and a ram speed of 2.1 mm/s. Figures 3(e, f) represent the grain structures resulting from the extrusion made with a billet temperature of 490 °C and a ram speed of 9.2 mm/s. Figures 3(g, h) represent the grain structures resulting from the extrusion made with a billet temperature of 490 °C and a ram speed of 10.4 mm/s. In Fig. 4(a), the microstructure of the billet is reported, with an average grain size of 137 μm. As clearly visible from the images, Figs. 3(a, b) present a partially recrystallized microstructure, while all other cases present a fully recrystallized grain structure. The predictions of the statically recrystallized grain dimensions will be made for the conditions shown in Figs. 3(c−h), where 100% (in the volume fraction) of static recrystallization occurred. For the extrusion performed at a ram speed of 1.1 mm/s, as shown in Figs. 3(a, b) with a partially recrystallized microstructure, the outcomes of the recrystallization thickness prediction and the utilization of a previously validated model from [5] for estimating the dimensions of fibrous grains will be presented. In the 2.1 mm/s ram speed case, the grains in the centre of the profile are significantly bigger than the ones near the external surface, while in the 9.2 and 10.4 mm/s cases, the grain size is finer and more homogeneous through the profile area. Twenty points were chosen for measurement for each acquired microstructure: at each point, the grain

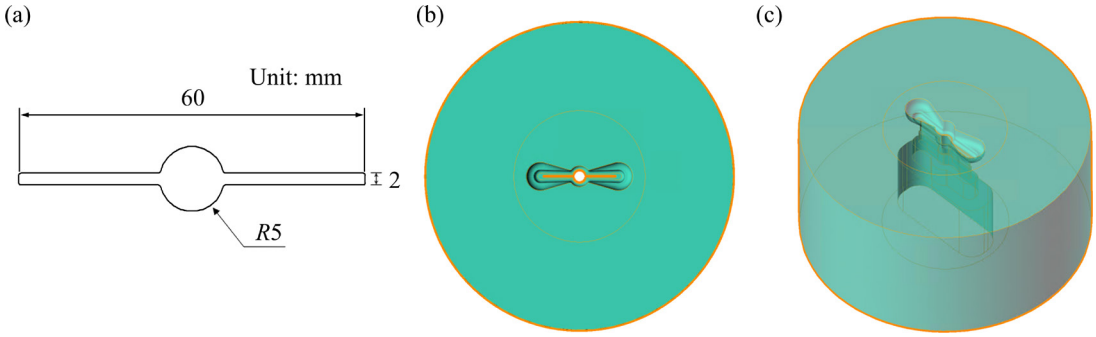

Fig. 2 Investigated profiles and die geometries: (a) Profile geometry; (b, c) Die geometry (from CAD)

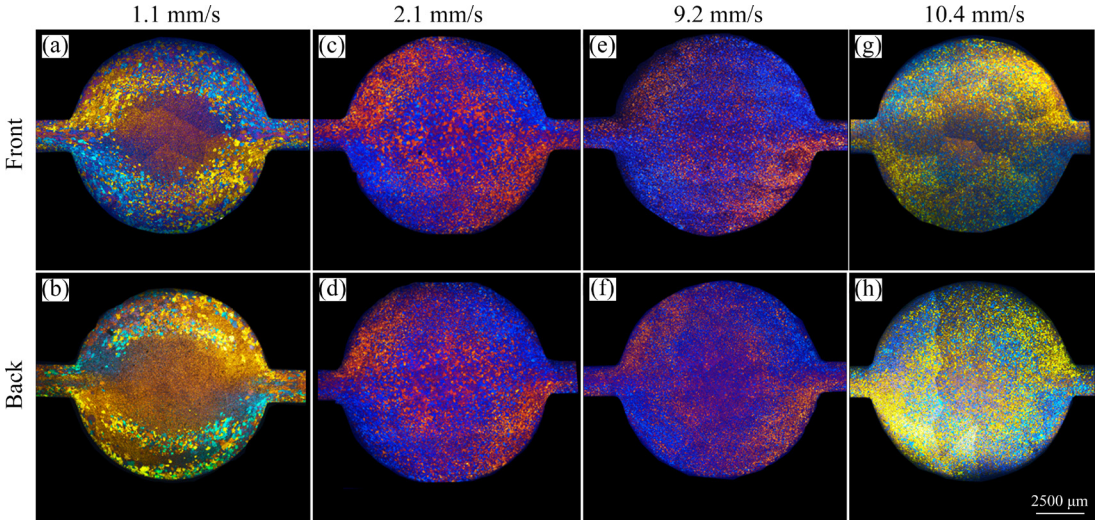

Fig. 3 Microstructures of Hydro extruded profiles

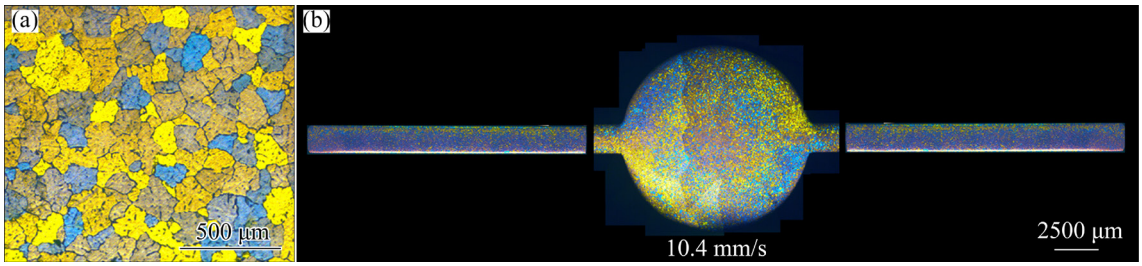

Fig. 4 Microstructure of billet (a) and entire Hydro profile (b)

size was measured according to the ASTM-E112 regulation using the ImageJ software. Ten of these measurements were used as calibration data in order to optimize the recrystallization model. The other ten measurements were used to check the model's accuracy by comparing the data with the results of the numerical prediction.

All the process and experimental parameters were summarized in Table 1.

Table 1 Process parameters

Process parameter	Description or value
Material	AA6063
Extrusion ratio	46
Ram speed/(mm·s^{-1})	1.1, 2.1, 9.2, 10.4
Container temperature/°C	400
Billet temperature/°C	420, 490
Die temperature/°C	400
Ram acceleration time/s	5
Billet length/mm	270
Billet diameter/mm	100
Container diameter/mm	107
Billet rest length/mm	15

In order to ensure the reliability of the model, the results of the recrystallization prediction were validated on two other industrial-size AA6063 profiles, A and B, presented below. The data on the grain size of Profile A were taken from the work of GAMBERONI et al [28], while for Profile B, they were experimentally acquired. The two extrusions reveal different characteristics in terms of temperatures, profile shapes, dimensions, and extrusion ratios, thus producing a wide amount of data for the numerical model validation. In detail, Profile A is characterized by an extrusion ratio of 10, a ram speed of 8.5 mm/s and billet temperature of 470 °C, while Profile B is characterized by an extrusion ratio of 44, a ram speed of 6.4 mm/s and a billet temperature of 530 °C.

In Fig. 5, the geometries of the Profiles A and B are reported together with the CAD image of the dies and the microstructures obtained from the experimental analysis. All the investigated samples were acquired once the extrusion process had achieved the thermal steady-state condition. As for Profile A, the micrograph reported in Fig. 5(c) reveals a completely recrystallized microstructure within a minimum grain dimension of 55 μm. The maximum grain dimension (around 500 μm) is detectable where the profile shows PCG and AGG (abnormal grain growth) structures. These structures are characterized by coarse grains with respect to the dimension of the surrounding grains, which may reduce crash, mechanical, corrosion, and fracture properties. The microstructure of Profile B is shown in Fig. 5(f). The figure shows a completely recrystallized structure within an average dimension range of 40−170 μm.

4 Recrystallization model

4.1 SRX

The static recrystallization of a 6xxx aluminum alloy was predicted according to the model proposed by VATNE et al [14] and further investigated by NEGOZIO et al [27]. The model allows the prediction of the static recrystallized grain size (D_{rex}) due to the contribution of three nucleation components N_{PSN}, N_{GB} and N_C:

$$D_{rex}=DN^{-1/3} \quad (1)$$

$$N=N_{PSN}+N_{GB}+N_C \quad (2)$$

where D is a material parameter and N is the total nucleation density.

According to VATNE et al [14], these three contributions were calculated as follows:

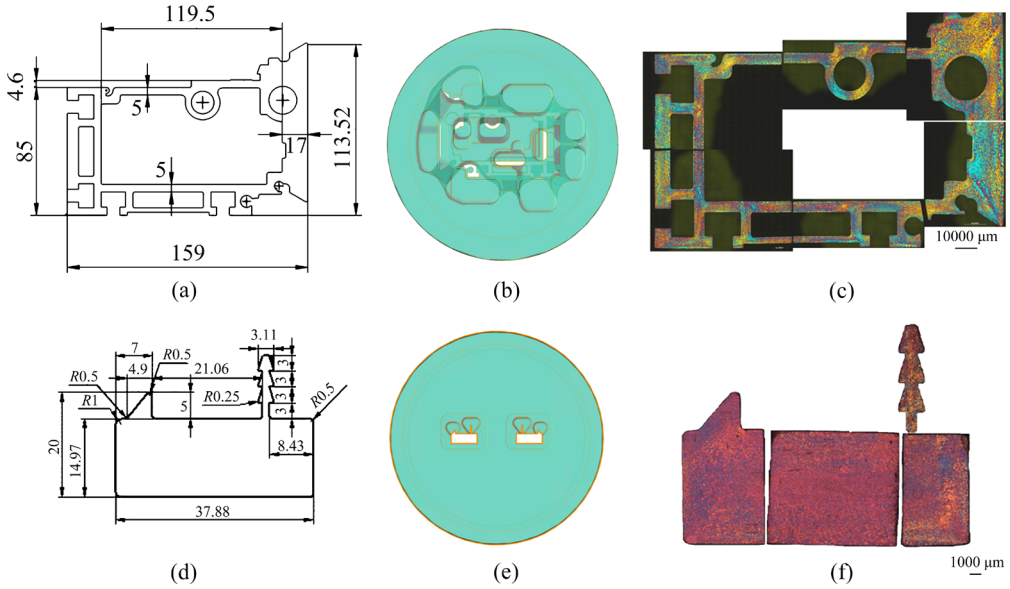

Fig. 5 Investigated profiles (unit: mm) (a, d), top view of CAD die (b, e) and microstructure (c, f): (a−c) Profile A; (d−f) Profile B

$$N_{PSN}=C_{PSN}\exp\left(\frac{-A_{PSN}}{P_d-P_z}\right) \tag{3}$$

$$N_{GB}=C_{GB}\delta A(\varepsilon)S_{GB} \tag{4}$$

$$N_C=C_C\delta A(\varepsilon)S_C \tag{5}$$

where δ is the subgrain size, $A(\varepsilon)$ is the grain boundary area per volume at a given strain, S_{GB} and S_C are the numbers of subgrains larger than a critical subgrain size δ^* ($S_{GB}=S_C$ [14]). C_{PSN}, A_{PSN}, C_{GB} and C_C are the material parameters required to optimize the model for each specific 6xxx alloy.

The stored energy (P_d) and the Zener Drag pressure (P_z), which represent the driving and the retarding force for the recrystallization [29], respectively, were calculated according to SELLARS and ZHU [13] and HUMPHREYS and HATHERLY [30]:

$$P_d=\frac{Gb^2}{10}\left[\rho_i\left(1-\ln\left(10b\rho_i^{0.5}\right)\right)+\frac{2\theta}{b\delta}\left(1+\ln\left(\frac{\theta_c}{\theta}\right)\right)\right] \tag{6}$$

$$P_z=\frac{3f\gamma}{4r} \tag{7}$$

where G is the shear modulus of material (2.05×10^{10} Pa), b the magnitude of Burgers vector (2.86×10^{-10} m), ρ_i is the internal dislocation density, δ is the subgrain size, θ is the subgrain misorientation angle, and θ_c is the misorientation angle limit (15°). In the Zener Drag pressure calculation (Eq. (7)), f and r are the fraction area and the mean size of the dispersoids, respectively, and γ is the grain boundary energy (0.3 J/m^2 [27]). In this work, values for f and r were taken from REMØE et al [31], where the microstructure of different 6xxx alloys were analysed. For the AA6063 aluminum alloy, the analysis reports an average value of 0.023% for the fraction area and around 60 nm for the mean size of the dispersoids.

The internal dislocation density (ρ_i) and the subgrain misorientation angle (θ) were taken from NEGOZIO et al [27], where are considered as functions of the Zener−Hollomon parameter (Z) and strain (ε). In that work, the experimental data on the evolution of the internal dislocation density (ρ_i) and the subgrain misorientation angle θ were presented and used to calculate the stored energy. In the current work, two new empirical equations for the computation of ρ_i (Eq. (8)) and θ (Eq. (9)) were proposed and calibrated by curve fitting method using experimental data presented in previously mentioned work [27]. Consequently, the equations material parameters (C_1, C_2, C_3 in Eq. (8) and C_4, C_5, C_6 in Eq. (9)) were found, and the behaviour of two parameters in relation to Zener−Hollomon parameter is reported in Fig. 6.

$$\rho_i=(C_1\cdot Z^{C_2})\cdot[1-\exp(C_3\cdot\varepsilon)] \tag{8}$$

$$\theta=(C_4\cdot Z^{C_5})\cdot[1-\exp(C_6\cdot\varepsilon)] \tag{9}$$

where C_1=328157965, C_2=0.27, C_3=−5, C_4=0.85, C_5=0.05, and C_6=−2.5.

According to Ref. [5], the subgrain size (δ) and the Zener−Hollomon parameter (Z) were calculated:

$$\frac{1}{\delta}=C(\ln Z)^n \tag{10}$$

$$Z=\dot{\varepsilon}\exp\left(\frac{Q}{RT}\right) \tag{11}$$

where C=3.36×10^{-9} m^{-1}, n=5.577, Q is activation energy of the AA6063 (232350 J/(mol·K) [28]), R is the molar gas constant (8.341 J/mol), and $\dot{\varepsilon}$ is the maximum strain rate that the analyzed point experiences in its flow path during extrusion. This maximum value was calculated by a developed user-subroutine in order to overcome the limit represented by the standard result of the strain rate simulation. In fact, the typical FEM results of the strain rate values calculated in the profile cross-section (immediately after the bearing zone) are always nearby zero (Fig. 7(b)). The comparison between the strain rate values evaluated by using the innovative approach and the standard Qform UK results are reported in Fig. 7.

$A(\varepsilon)$ represents the boundary surface per volume at a certain value of strain and S_{GB} corresponds to the subgrain which has a dimension higher than a critical subgrain size δ^*. These values are calculated according to Refs. [15,27]:

$$\delta^*=\frac{4\gamma}{P_d-P_z} \tag{12}$$

$$A(\varepsilon)=\frac{1}{D_0}[p_1-p_2\exp(p_3\,\varepsilon^{p_4})] \tag{13}$$

where D_0 is the billet grain size, and p_1, p_2, p_3 and p_4 are constants (p_1=1.90, p_2=1.06, p_3=exp(−7), and p_4=6.00 [27]).

4.2 DRX

The grain size immediately after the extrusion process, before the occurrence of the static recrystallization, was calculated [5]:

$$d_t=(d_0-2.5\delta_{ss})\cdot k_1^{\bar{\varepsilon}}+2.5\delta_{ss} \tag{14}$$

$$d_l=k_2\bar{\varepsilon}^2-k_3\bar{\varepsilon}+d_0 \text{ if } \varepsilon<\varepsilon_p \tag{15}$$

$$d_l=k_4\bar{\varepsilon}^{-m}+10\delta_{ss} \text{ if } \varepsilon>\varepsilon_p \tag{16}$$

where d_t and d_l represent the thickness and length of the dynamically recrystallized grain, respectively, ε_p is the critical pinch-off strain (ε_p=3 [5]), δ_{ss} is the subgrain size at the steady-state condition (δ_{ss}=8.4 μm [5]), and m, k_1, k_2, k_3 and k_4 are material constants (m=4.75, k_1=0.4, k_2=85.192, k_3=14.88, and k_4=1.68×10^5 [5]).

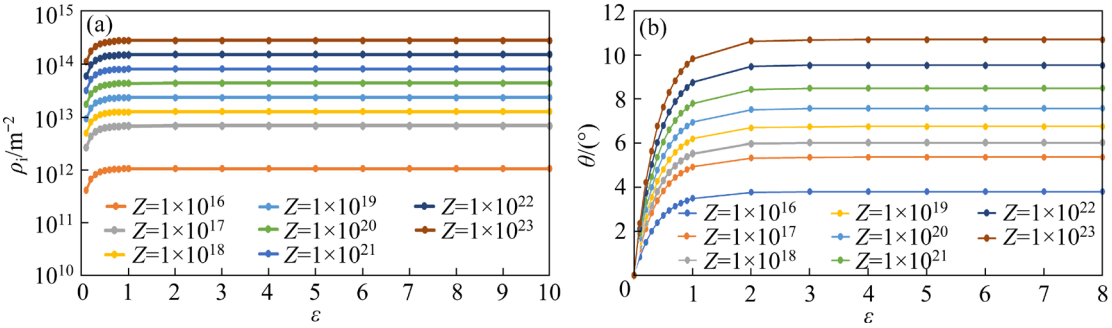

Fig. 6 Internal dislocation density (a) and subgrain misorientation angle (b) as function of Zener−Hollomon parameter (Z) and strain (ε)

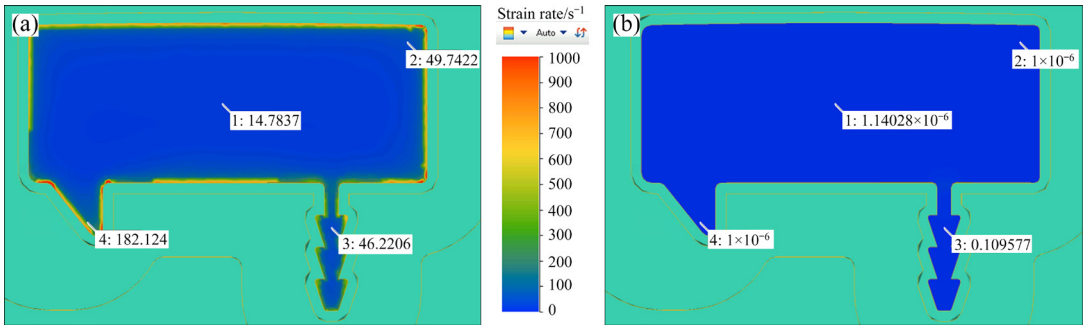

Fig. 7 Comparison between strain values calculated according to proposed subroutine (max strain rate values during the material path) (a) and Qform standard output (b)

5 FEM simulations

Qform Extrusion® was used to perform the simulations of the investigated process. This software is an Arbitrarian Lagrangian Eulerian FEM code optimized for the simulation of the hot extrusion. The following simulation parameters were considered:

(1) According to Ref. [27], the sticking friction condition was applied to the billet-die/ram/container interfaces, while a Levanov friction model with m=0.3 and n=1.25 was applied to the bearing zone.

(2) The material parameters for the AA6063 aluminum alloy were taken from the Qform material database.

(3) Hensel−Spittel plastic flow constitutive model [27] was used (Eq. (17)), where $\bar{\sigma}$ is the flow stress, $\bar{\varepsilon}$ is the strain, $\dot{\bar{\varepsilon}}$ is the strain rate, and T is the temperature (K). The Hensel−Spittel material coefficients are reported in Table 2 [32].

$$\bar{\sigma}=A\cdot\exp(m_1T)\cdot\bar{\varepsilon}^{m_2}\cdot\dot{\bar{\varepsilon}}^{m_3}\cdot\exp(m_4/\bar{\varepsilon})\cdot(1+\bar{\varepsilon})^{m_5T}\cdot\exp(m_7\bar{\varepsilon})\cdot\dot{\bar{\varepsilon}}^{m_8T}\cdot T^{m_9} \quad (17)$$

The predicted extrusion load and the exit temperature of the profiles were further compared to the ones experimentally acquired in order to validate the simulation outputs. In Table 3 and Fig. 8, the results of the simulation of Profile Hydro are reported, showing the good accuracy of the simulations. A similar precision was found for the numerical analysis of all the other process conditions in Profile Hydro, Profile A and Profile B.

The strain, strain rate, and temperature variables were calculated using FEM simulation. These values were used in the post-processing analysis as input data for the calculation of the final grain size of the profile. The material constants for the 6xxx recrystallization model were calculated using an optimization approach that made use of both the results of the FEM simulation and the acquired experimental data. These constants given in Table 4 were computed by using the Levenberg−Marquardt non-linear regression algorithm [33]. After this calculation, the model was implemented in a user subroutine within the Qform extrusion environment for the recrystallization analysis. Using the developed routine, the model was run in post-processing, with the output of the extrusion simulation as input data for the recrystallization analysis.

Table 2 Hensel−Spittel material coefficients for AA6063 aluminum alloy [32]

Parameter	Value
A/MPa	1014.7
m_1/K^{-1}	−0.00438
m_2	0.2425
m_3	−0.0965
m_4	−0.000438
m_5/K^{-1}	−0.000766
m_7	0.002939
m_8/K^{-1}	0.000291
m_9	0

6 Results and discussion

6.1 DRX

Figures 9 and 10 illustrate a comparison between experimental and numerical grain sizes after dynamic recrystallization immediately after the bearing zone. Figures 9(a, c) present the numerical results compared with experimental data (Figs. 9(b, d)), as well as the data in Fig. 10. Randomly selected points within the fibrous region of the analyzed profile, corresponding to the inner part of the profile extruded with a ram speed of 1.1 mm/s, were used for comparison of both numerical and experimental data. Both numerical and experimental data were compared and collected in the graph shown in Fig. 10(a) (for the grain

Table 3 Comparison between experimental and numerical peak loads and profile exit temperatures

Condition	Peak load/MN			Exit temperature/°C		
	Experimental	Numerical	Error	Experimental	Numerical	Error
Low ram speed	3.47	3.20	0.27	433	438	5
High ram speed	4.77	4.64	0.13	551	546	5

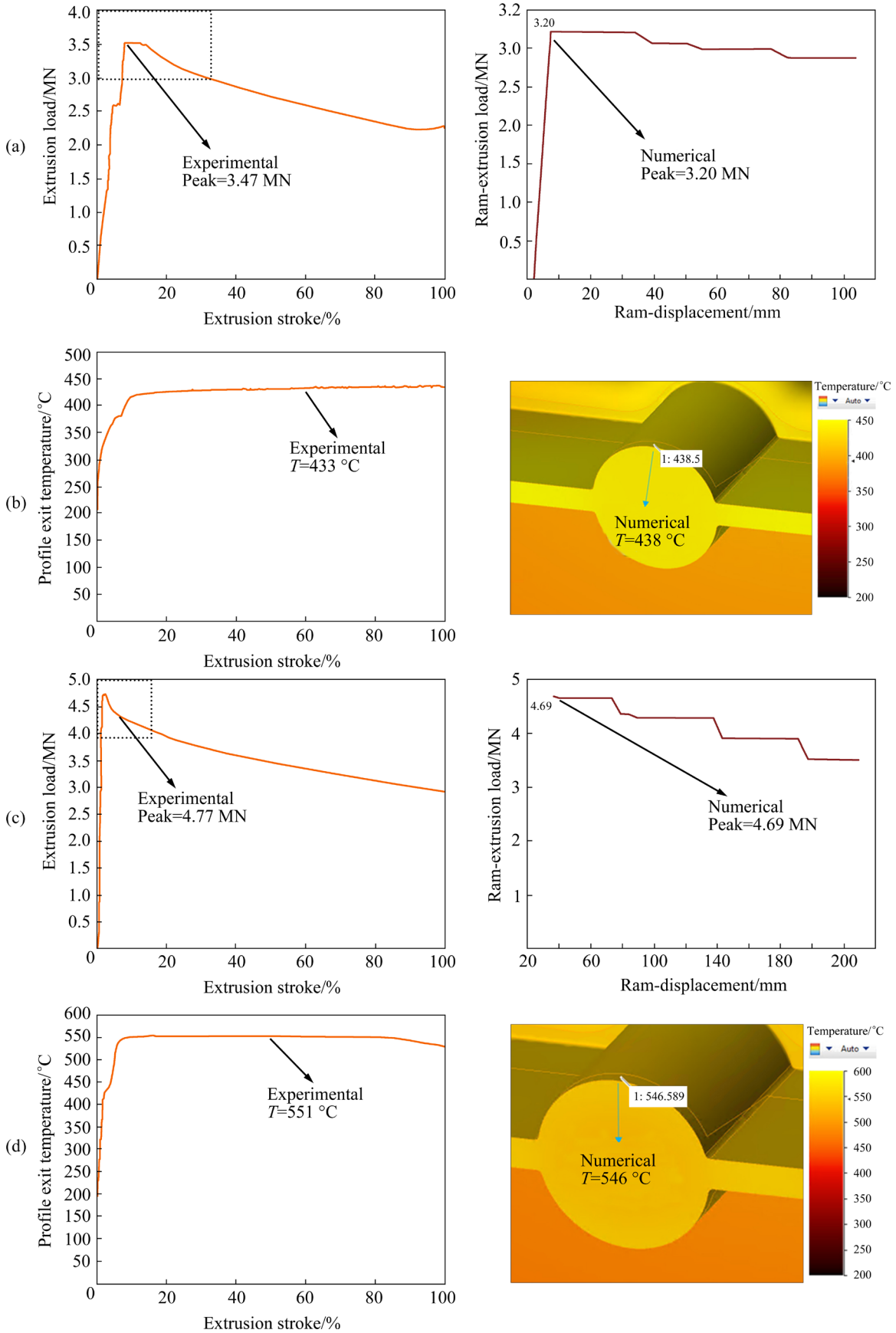

Fig. 8 Profile Hydro simulation: (a, b) Comparison between experimental and numerical extrusion load and exit temperature in extrusion with ram speed of 1.1 mm/s; (c, d) Comparison between experimental and numerical extrusion load and exit temperature in extrusion with ram speed of 10.4 mm/s

Table 4 Recrystallization model material constants of AA6063

Material constant	AA6063
C_{PSN}	4.99824e^{13}
A_{PSN}	864753
C_{GB}	0.00022279
C_C	0.00022279

thickness prediction) and Fig. 10(b) (for the grain length prediction). In Fig. 10, the x-axis and the y-axis represent the experimental and numerical dimensions of the grain size, respectively. Consequently, the red 45° line corresponds to 100% matching between numerical and experimental values. In addition, two green lines corresponding to an error of 25% were reported. 25% was selected as the error range considering both the high number of metallurgical and process factors that affect the final grain size and the approximations derived from the measurement methodology chosen for the experimental analysis of the average grain diameter. For these reasons, this range, also used by DONATI et al [5] for the investigation of a laboratory-scale extruded profile microstructure prediction, is considered an excellent accuracy range. As evidenced by the graphs in Figs. 10(a) and (b), 100% of the points are within the 25%

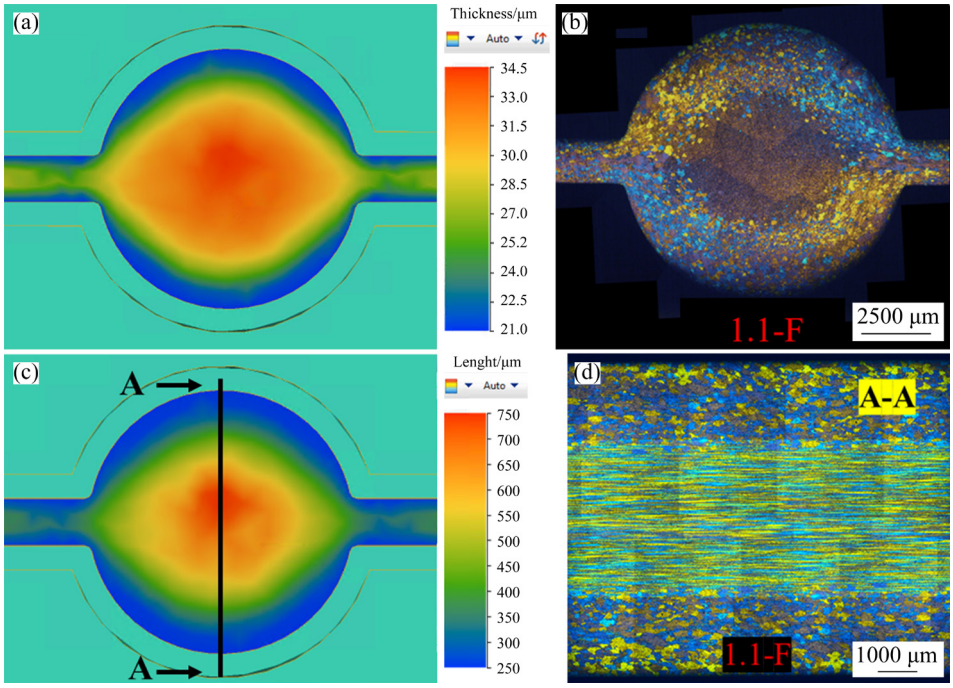

Fig. 9 Profile Hydro: (a) Numerical grain thickness; (b) Experimental microstructure (cross section); (c) Numerical grain length; (d) Experimental microstructure (longitudinal section)

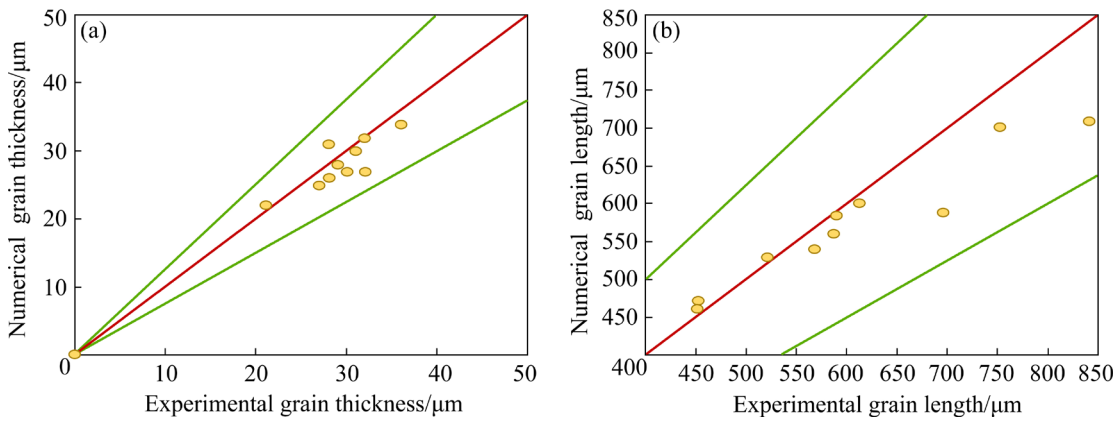

Fig. 10 DRX analysis: (a) Comparison between experimental and numerical grain thickness of Profiles Hydro; (b) Comparison between experimental and numerical grain length of Profile Hydro

error lines for both the prediction of length and thickness of the fibrous grains, thus confirming the model reliability for dynamic recrystallization evaluation.

6.2 SRX

In Fig. 11, the outputs of the simulation involving the prediction of recrystallized layer thickness are reported and compared to the experimental microstructures. The area in red indicates the part of the profile where the static recrystallization occurred, while the area in blue indicates where the grain structure remains fibrous. Since the microstructure of the "front" samples is almost the same as the "back" samples (Fig. 3), only the images of the "front" part are reported for the comparison. In AA6063 aluminum alloy, due to a low or absent dispersoid concentration [4], SRX is extremely likely to occur after the profile exits the die. Consequently, all the investigated profiles present a completely recrystallized structure except the one extruded at the lowest speed (Fig. 11(a)), which is only partially recrystallized. In such a case, the simulation reports, in agreement with the experimental evidence, a partially recrystallized microstructure (Fig. 11(b)). In all the remaining cases, in accordance with the experimental evidence, the computed/modeled microstructure is completely recrystallized.

After the SRX thickness investigation, a comparison between the predicted and experimental grain sizes was carried out. In Fig. 12, the data

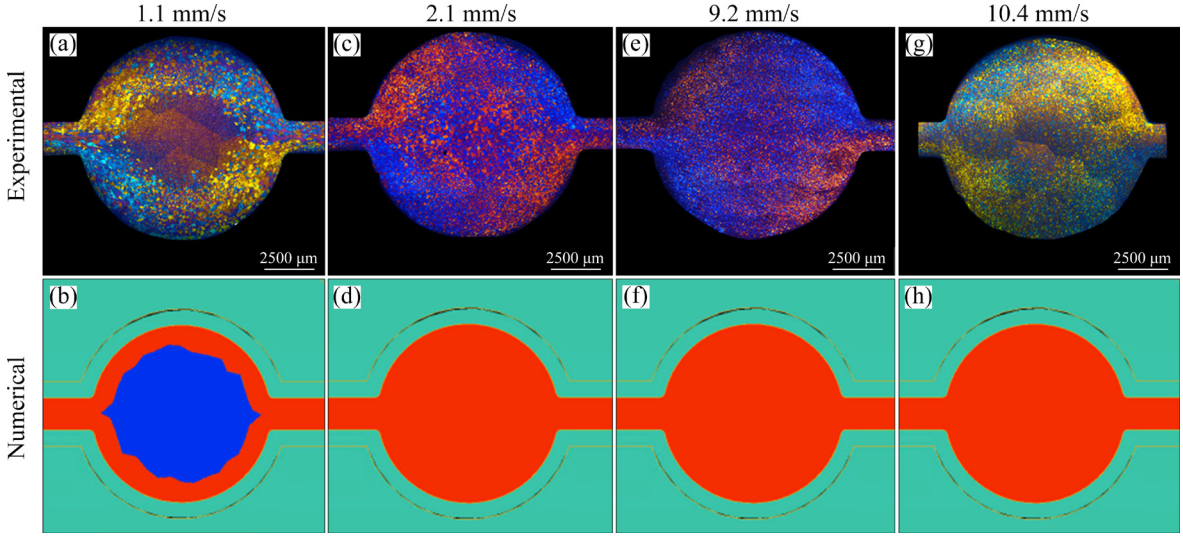

Fig. 11 Recrystallization thickness analysis (Red area: SRX area; Blue area: No SRX area)

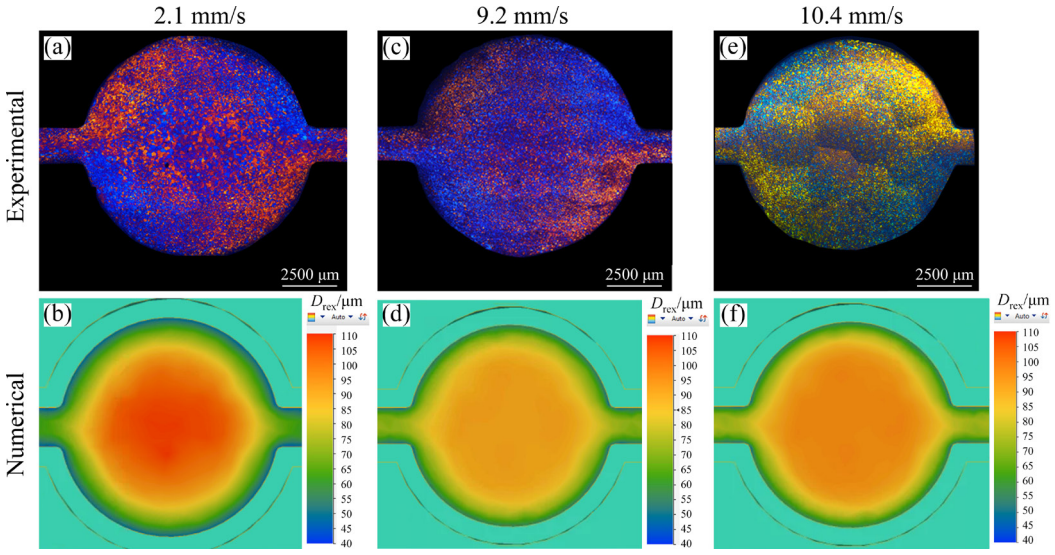

Fig. 12 Grain size analysis after SRX

about Profile Hydro are reported. The images shown with each microstructure (Figs. 12(b, d, f)) report the results of the grain size prediction simulation. In these figures, the values of the average diameter are reported, with a scale bar ranging from 40 μm (blue) to 110 μm (red). The numerical predictions show that the sample extruded with a ram speed of 2.1 mm/s presents the coarser grain size in the inner area (Fig. 12(b)), while the sample extruded with a ram speed of 9.2 mm/s has smaller one (Fig. 12(d)), in accordance with the experimental tests, thus proving the stability of the numerical computation.

In order to illustrate the accuracy of the prediction using developed AA6063 recrystallization model, Figs. 13 and 14 show qualitative and quantitative comparison between the numerical and experimental grain sizes of Profile Hydro extruded with ram speeds of 2.1 and 9.2 mm/s in three between the set of validation points. Figures 13 and

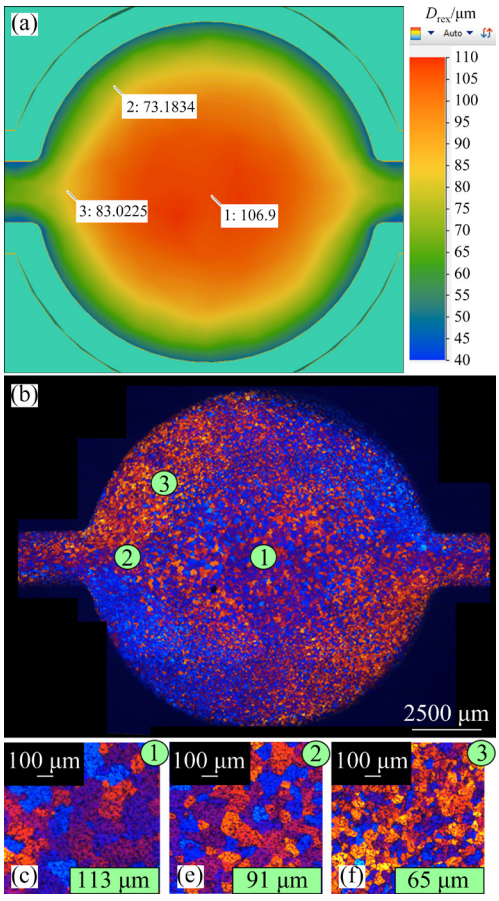

Fig. 13 Comparison between experimental and numerical grain size of Profile Hydro extruded with ram speed of 2.1 mm/s: (a) Numerical results; (b) Experimental results; (c) Microstructure of Zone 1; (d) Microstructure of Zone 2; (e) Microstructure of Zone 3

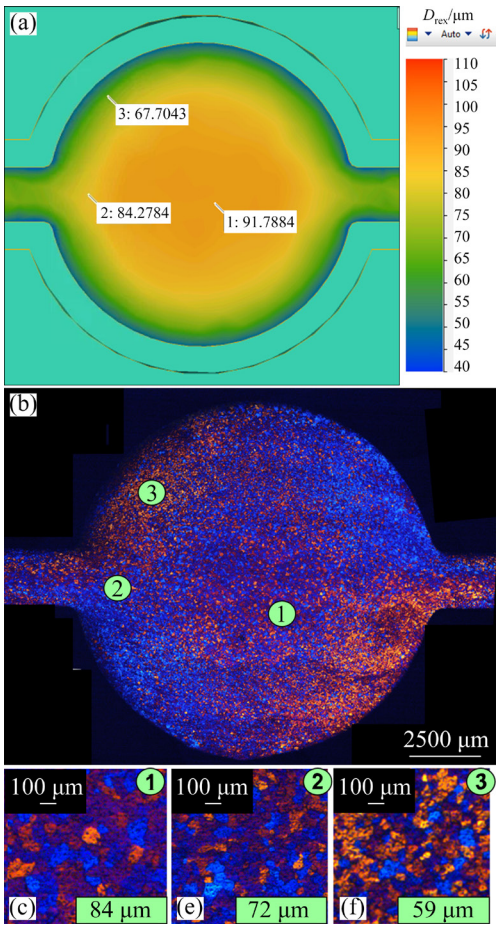

Fig. 14 Comparison between experimental and numerical grain size of Profile Hydro extruded with ram speed of 9.2 mm/s: (a) Numerical results; (b) Experimental results; (c) Microstructure of Zone 1; (d) Microstructure of Zone 2; (e) Microstructure of Zone 3

14 demonstrate that the recrystallization model provides an reliable estimation of the average grain size under varying process conditions. Notably, from an experimental perspective, it is apparent that adjustments in the extrusion velocity and, subsequently, the process strain-rate, lead to observable size variations in the central region of the Profile Hydro. Specifically, when the ram speed is set at 2.1 mm/s, a larger grain size is observed in contrast to the condition with a ram speed of 9.2 mm/s. This variation is correctly replicated by the simulation, as depicted in Figs. 13 and 14, which predict a reduced maximum grain size in the case of extrusion at 9.2 mm/s, as opposed to 2.1 mm/s.

The grain size prediction was also carried out both for Profile A and Profile B using the same numerical model. The comparison between

numerical and experimental diameters of the recrystallized grain for Profiles Hydro, A and B is reported in Fig. 15. A representative number of points taken randomly from the profiles investigated were selected, where blue dots highlight the points taken from PCG/AGG areas. If the blue dots are excluded from the analysis, almost the whole sampling/population (over 90% if the PCG/AGG points are not excluded) is within the 25% error, thus proving the good accuracy and excellent reliability of the numerical model for the grain size prediction.

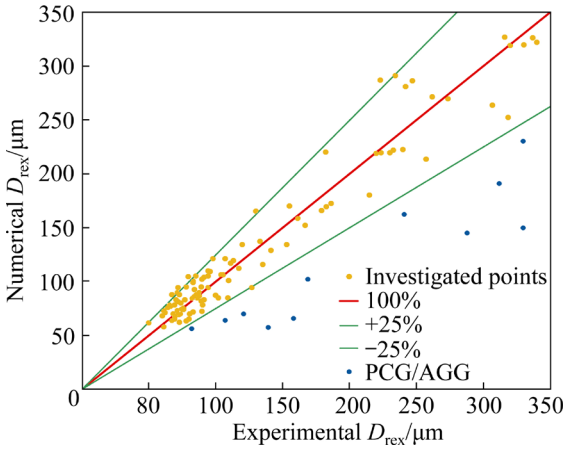

Fig. 15 Comparison between experimental and numerical grain size of Profiles Hydro, A and B

7 Conclusions

(1) An extensive analysis of three AA6063 aluminum alloy profiles, including variations in ram speeds and billet temperatures, provided the data required for calibrating the recrystallization model. Additionally, microstructural data from two industrial-scale AA6063 aluminum alloy profiles were considered to validate the model.

(2) The study introduced a novel approach to developing a recrystallization model for 6xxx alloys. This method employed a regression-based technique to determine the material constants, addressing limitations and errors associated with existing literature assumptions. Notably, two new equations were proposed for calculating the internal dislocation density and the subgrain misorientation angle. The model was calibrated using experimental data on grain size for AA6063 aluminum alloys, enabling accurate predictions of recrystallization layer thickness and final grain size after dynamic and static recrystallization.

(3) The model developed using the proposed methodology demonstrated the good agreement between experimental and numerical results, specifically in predicting recrystallization thickness and grain size. This success underscores the model's reliability and robustness in forecasting microstructural evolution in AA6063.

CRediT authorship contribution statement

Marco NEGOZIO: Conceptualization, Methodology, Software, Validation, Formal analysis, Investigation, Writing − Original draft; **Antonio SEGATORI:** Methodology, Resources; **Riccardo PELACCIA:** Conceptualization, Writing − Review & editing, Visualization; **Barbara REGGIANI:** Formal Analysis, Data curation, Writing − Review & editing; **Sara Di DONATO:** Investigation, Visualization; **Lorenzo DONATI:** Conceptulization, Methodology, Supervision, Project administration.

Declaration of competing interest

The authors declare that they have no known competing financial interests or personal relationships that could have appeared to influence the work reported in this paper.

References

[1] LI Shi-kang, LI Luo-xing, HE Hong, LIU Zhi-wen, ZHANG Long. Influence of dynamic recrystallization on microstructure and mechanical properties of welding zone in Al−Mg−Si aluminum profile during porthole die extrusion [J]. Transactions of Nonferrous Metals Society of China, 2019, 29(9): 1803−1815. https://doi.org/10.1016/S1003-6326(19)65088-0.

[2] HU Cheng-liang, MENG Li-fen, ZHAO Zhen, GU Bing, CAI Bing. Optimization for extrusion process of aluminum controller housing [J]. Transactions of Nonferrous Metals Society of China, 2012, 22(1): 48−53. https://doi.org/10.1016/S1003-6326(12)61682-3.

[3] DONATI L, REGGIANI B, PELACCIA R, NEGOZIO M, DI DONATO S. Advancements in extrusion and drawing: A review of the contributes by the ESAFORM community [J]. International Journal of Material Forming, 2022, 15(6): 41. https://doi.org/10.1007/s12289-022-01664-w.

[4] LIU Ru-xue, LI Kai, ZHOU Guo-wei, TANG Wei-qin, SHEN Yao, TANG Ding, LI Da-yong. Simulation of strain induced abnormal grain growth in aluminum alloy by coupling crystal plasticity and phase field methods [J]. Transactions of Nonferrous Metals Society of China, 2022, 32(12): 3873−3886. https://doi.org/10.1016/S1003-6326(22)66064-3.

[5] DONATI L, SEGATORI A, EL MEHTEDI M, TOMESANI L. Grain evolution analysis and experimental validation in

the extrusion of 6XXX alloys by use of a Lagrangian FE code [J]. International Journal of Plasticity, 2013, 46: 70−81. https://doi.org/10.1016/j.ijplas.2012.11.008.

[6] CHEN Shuai-feng, LI Da-yong, ZHANG Si-Hai, HAN Heung-nam, LEE Ho-won, LEE Myoung-gyu. Modelling continuous dynamic recrystallization of aluminum alloys based on the polycrystal plasticity approach [J]. International Journal of Plasticity, 2020, 131: 102710. https://doi.org/10.1016/j.ijplas.2020.102710.

[7] CHEN Fei, TIAN Xiao, WU Guang-shan, ZHU Hua-jia, OU Hen-gan, CUI Zhen-shan. Coupled quantitative modeling of microstructural evolution and plastic flow during continuous dynamic recrystallization [J]. International Journal of Plasticity, 2022, 156: 103372. https://doi.org/10.1016/j.ijplas.2022.103372.

[8] MCQUEEN H J, KNUSTAD O, RYUM N, SOLBERG J K. Microstructural evolution in Al deformed to strains of 60 at 400 °C [J]. Scripta Metallurgica, 1985, 19(1): 73−78. https://doi.org/10.1016/0036-9748(85)90268-6.

[9] GOURDET S, MONTHEILLET F. A model of continuous dynamic recrystallization [J]. Acta Materialia, 2003, 51: 2685−2699. https://doi.org/10.1016/S1359-6454(03)00078-8.

[10] TIAN Xiao, CHEN Fei, JIANG Jun-nan, WU Guang-shan, CUI Zhen-shan, QIAN Dong-sheng, HAN Xing-hui, WANG Bin, WANG Heng-qiang, WANG He, LIU Pan. Experimental analyses and numerical modeling of the microstructure evolution of aluminum alloy using an internal state variable plasticity-based approach coupled with the effects of second phase [J]. International Journal of Plasticity, 2022, 158: 103416. https://doi.org/10.1016/j.ijplas.2022.103416.

[11] de PARI Luigi, MISIOLEK W. Theoretical predictions and experimental verification of surface, grain structure evolution for AA6061 during hot rolling [J]. Acta Materialia, 2008, 56: 6174−6185. https://doi.org/10.1016/j.actamat.2008.08.050.

[12] SCHIKORRA M, DONATI L, TOMESANI L, TEKKAYA A E. Microstructure analysis of aluminum extrusion: Prediction of microstructure on AA6060 alloy [J]. Journal of Materials Processing Technology, 2008, 201(1/2/3): 156−162. https://doi.org/10.1016/j.jmatprotec.2007.11.160.

[13] SELLARS C M, ZHU Qin-shu. Microstructural modelling of aluminium alloys during thermomechanical processing [J]. Materials Science and Engineering A, 2000, 280: 1−7. https://doi.org/10.1016/S0921-5093(99)00648-6.

[14] VATNE H E, FURU T, ORSUND R, NES E. Modelling recrystallization after hot deformation of aluminum [J]. Acta Materialia, 1996, 11: 4463−4473. https://doi.org/10.1016/1359- 6454(96)00078-X.

[15] EIVANI A R, ZHOU J, DUSZCZYK J. Grain boundary versus particle stimulated nucleation in hot deformed Al−4.5Zn−1Mg alloy [J]. Materials Science and Technology, 2013, 29: 517−528. https://doi.org/10.1179/1743284712Y.0000000176.

[16] HE You-feng, XIE Shui-sheng, CHENG Lei, HUANG Guo-jie, FU Yao. FEM simulation of aluminum extrusion process in porthole die with pockets [J]. Transactions of Nonferrous Metals Society of China, 2010, 20(6): 1067−1071. https://doi.org/10.1016/S1003-6326(09)60259-4.

[17] HE Zhao, WANG He-nan, WANG Meng-jun, LI Guang-yao. Simulation of extrusion process of complicated aluminium profile and die trial [J]. Transactions of Nonferrous Metals Society of China, 2012, 22(7): 1732−1737. https://doi.org/10.1016/S1003-6326(11)61380-0.

[18] FERESHTEH-SANIEE F, FAKHAR N, KARIMI M. Experimental, analytical, and numerical studies on the forward extrusion process [J]. Materials and Manufacturing Processes, 2013, 28(3): 265−270. https://doi.org/10.1080/10426914. 2012.689454.

[19] YI Jie, WANG Zhen-hu, LIU Zhi-wen, ZHANG Jian-ming, HE Xin. FE analysis of extrusion defect and optimization of metal flow in porthole die for complex hollow aluminium profile [J]. Transactions of Nonferrous Metals Society of China, 2018, 28(10): 2094−2101.

[20] YI Jie, LIU Zhi-wen, ZENG Wen-qi. Isothermal extrusion speed curve design for porthole die of hollow aluminium profile based on PID algorithm and finite element simulations [J]. Transactions of Nonferrous Metals Society of China, 2021, 31(7): 1939−1950.

[21] ZHANG Kai, MARTHINSEN K, HOLMEDAL B, AUKRUST T, SEGATORI A. Through thickness variations of deformation texture in round profile extrusions of 6063-type aluminium alloy: Experiments, FEM and crystal plasticity modelling [J]. Materials Science and Engineering A, 2018, 722: 20−29. https://doi.org/10.1016/j.msea.2018.02.081.

[22] KHAN A S, LIU Jian, YOON J W, NAMBORI R. Strain rate effect of high purity aluminum single crystals: Experiments and simulations [J]. International Journal of Plasticity, 2015, 67: 39−52. https://doi.org/10.1016/j.ijplas.2014.10.002.

[23] PELACCIA R, REGGIANI B, NEGOZIO M, DONATI L. Liquid nitrogen in the industrial practice of hot aluminium extrusion: experimental and numerical investigation [J]. Int J Adv Manuf Technol, 2022, 119(4): 1−15. https://doi.org/10.1007/s00170-021-08422-3.

[24] EIVANI A R, ZHOU Ji. Application of physical and numerical simulations for interpretation of peripheral coarse grain structure during hot extrusion of AA7020 aluminum alloy [J]. Journal of Alloys and Compounds 2017, 725: 41−53. https://doi.org/10.1016/j.jallcom.2017.06.297.

[25] EIVANI A R, JAFARIAN H R, ZHOU Ji. Simulation of peripheral coarse grain structure during hot extrusion of AA7020 aluminum alloy [J]. Journal of Manufacturing Processes, 2020, 57: 881−892. https://doi.org/10.1016/j.jmapro.2020.07.011.

[26] MAHMOODKHANI Y, CHEN J, WELLS M, POOLE W J, PARSON N. The effect of die bearing geometry on surface recrystallization during extrusion of an Al−Mg−Si−Mn alloy [J]. Metallurgical and Materials Transactions A, 2019, 50: 5324−5335. https://doi.org/10.1007/s11661-019-05437-0.

[27] NEGOZIO M, PELACCIA R, DONATI L, REGGIANI B, DI DONATO S. Experimental analysis and modeling of the recrystallization behaviour of a AA6060 extruded profile [C]// Materials Research Proceedings 2023, Millersville PA, USA, 2023: 477−486. https://doi.org/10.21741/9781644902479-52.

[28] GAMBERONI A, DONATI L, REGGIANI B, HAASE M, TOMESANI L, TEKKAYA A E. Industrial benchmark 2015: Process monitoring and analysis of hollow EN AW-6063

extruded profile [C]// Materials Today: Proceedings 2015, UK, 2023: 4714−4725. https://doi.org/10.1016/j.matpr.2015.10.004.

[29] RIOS P, SICILIANO F, SANDIM H, LESLEY R, PADILHA A. Nucleation and growth during recrystallization [J]. Materials Research, 2005, 8(3): 225−238. https://doi.org/10.1590/S1516-14392005000300002.

[30] HUMPHREYS F J, HATHERLY M. Recrystallization and related annealing phenomena [M]. 2nd ed. Amsterdam: Elsevier, 2004.

[31] REMØE M S, WESTERMANN I, MARTHINSEN K. Characterization of the density and spatial distribution of dispersoids in Al−Mg−Si alloys [J]. Metals, 2019, 9(1): 26. https://doi.org/10.3390/met9010026.

[32] NEGOZIO M, PELACCIA R, DONATI L, REGGIANI B, PINTER T, TOMESANI L. Finite element model prediction of charge weld behaviour in AA6082 and AA6063 extruded profiles [J]. Journal of Materials Engineering and Performance, 2021, 30: 4691−4699. https://doi.org/10.1007/s11665-021-05752-x.

[33] GILL P E, MURRAY W. Algorithms for the solution of the nonlinear least-squares problem [J]. SIAM Journal on Numerical Analysis, 1978, 15(5): 977−992. https://doi.org/10.1137/0715063.

挤压过程中 AA6xxx 铝合金型材的再结晶行为模拟

Marco NEGOZIO[1], Antonio SEGATORI[2], Riccardo PELACCIA[3],
Barbara REGGIANI[3,4], Sara Di DONATO[5], Lorenzo DONATI[5]

1. University of Parma - Department of Engineering and Architecture,
Parco Area delle Scienze, 181/A, 43124 Parma, Italy;
2. Hydro, Innovation and Technology, Myrkärrsvägen 1, 612 31 Finspång, Sweden;
3. DISMI Department of Sciences and Methods for Engineering, University of Modena and Reggio Emilia,
Via Amendola 2, 42122, Reggio Emilia, Italy;
4. InterMech - MO.RE – University of Modena and Reggio Emilia, Piazzale Europa 1, Reggio Emilia 42124, Italy;
5. DIN Department of Industrial Engineering – University of Bologna, Viale Risorgimento 2, 40136, Bologna, Italy

摘　要：介绍了一种开发 AA6063 铝合金再结晶模型的创新方法。该方法结合了基于回归分析的材料常数测定技术，并引入了评估晶粒尺寸演变的新方程。该方法的校准和验证结合了从 3 种 AA6063 铝合金型材的挤压实验中获得的显微组织数据和使用 Qform Extrusion UK 有限元代码模拟的结果。结果表明，显微组织演化的实验结果与数值模拟的预测结果相吻合。该方法准确模拟了动态再结晶和静态再结晶后晶粒尺寸随不同工业参数变化的趋势，在几乎整个抽样计算中，误差都小于 25%。

关键词：再结晶模拟；铝合金挤压；有限元法；显微组织预测

(Edited by Bing YANG)